Fibers and Polymers 2003, Vol.4, No.4, 161-168

Analysis of the Dimensionless Torque in Cone Drum False Twisting Mechanism

Choon Gil Lee* and Tae Jin Kang[1]

Department of Textile and Fashion Technology, College of Engineering, Kyungil University, Kyungsan 712-701, Korea
[1]School of Materials Science and Engineering, Seoul National University, Seoul 151-742, Korea
(Received August 12, 2003; Revised December 1, 2003; Accepted December 8, 2003)

Abstract: An investigation of the dimensionless torque in the newly developed cone drum twister texturing mechanism is reported. The cone drum twister is one of the outer surface contacting friction-twisting devices in false-twist texturing. In this cone drum twister, a filament yarn passes over the surface of the cone drum that rotates by the passing yarn without a special driving device. This research is composed of the theoretical analysis of the false twisting mechanism and the experimental analysis at room temperature. The equations have been derived which shows interrelationship of the conical angle of cone drum, the wrapping angle, the drag angle, and the yarn helix angle. Theoretical values of dimensionless torque were calculated and were compared with the experimental results. It is shown that, as the conical angle and the projected wrapping angle increased, the dimensionless torque also increased. But the conical angle was reached to 30.75°, the dimensionless torque decreased.

Keywords: Dimensionless torque, Relative velocity of friction surface, Drag angle, Cone drum twister, Outer surface contacting friction-twisting device, Conical angle, Projected wrapping angle

Introduction

All kinds of conventional false twist methods have the drive systems for inserting twist to the filament yarns. The false twist methods have been used in synthetic fiber industry for the filament yarn texturing process. For the analysis of the false twist mechanism, several researchers have studied the false twist drive system experimentally and theoretically [1-6]. But the newly developed cone drum twister has no drive system for inserting false twist. The cone drum twister is one of the outer surface contacting friction-twisting devices in false-twist texturing.

The effects of heater temperature, linear density, draw ratio, projected wrapping angle, and conical angle on the false twisting tension and the yarn helix angle of the texturing yarns in the cone drum twister were studied experimentally in previous studies [7-9]. And the effects of heater temperature, linear density, draw ratio, and projected wrapping angle on the tenacity, crimp rigidity, skein shrinkage, breaking elongation of textured yarn produced by the cone drum twister were also studied experimentally in the above studies. And the effects of stud radius on dimensionless torque and physical properties of the textured yarns in the stud type cone drum twister also had been studied [10]. It showed that stud radius was a very important factor in the stud type cone drum texturing device. Also in addition the theoretical calculation of the relative velocity of friction surface of the system also had been studied [11]. The theoretical relations between the cone drum geometry and the yarn geometry, and especially to calculate the drag angle of the system also had been studied [12].

In the newly developed cone drum twister, the false twist is inserted on the twisting region by friction between the filament yarn and the rotating cone drum surface. Therefore, the cone drum twister is one of the outer surface contacting friction-twisting devices in false-twist texturing. In this cone drum twister, a filament yarn passes over the surface of the cone drum which is rotated by the passing yarn which is wrapped around the cone drum stud without a special driving device. Therefore this system is very simple compared with the conventional systems.

The purpose of this paper is to develop theoretical relations between the cone drum geometry and the yarn geometry, and especially to calculate the dimensionless torque of the system. The dimensionless torque of the cone drum twister is used to estimate the level of twist in yarns used in this apparatus.

Theoretical Analysis of Dimensionless Torque

Simplifications and Assumptions

Figure 1 shows the side view of the twist inserting drum of the newly developed cone drum type draw texturing apparatus. Our theoretical analysis of cone drum twister texturing process incorporates several simplifications and assumptions as follows:

1. The filament yarn path remains straight in the development figure of the false twisting contact region, i.e., the yarn lies on the shortest path in the false twisting contact region.
2. The angle of the false twist in the false twisting contact region is constant.
3. The coefficient of friction is constant and independent

*Corresponding author: cglee@kiu.ac.kr

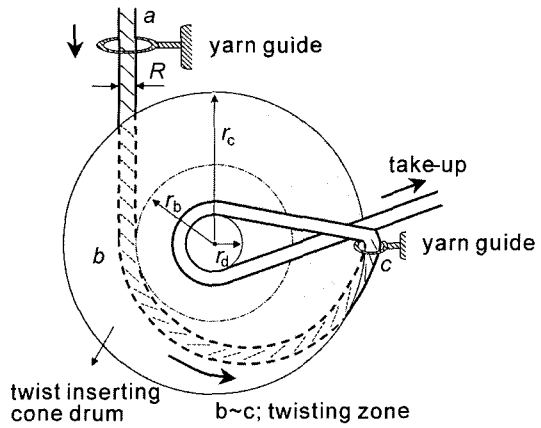

Figure 1. Side view of the twist inserting drum of the newly developed cone drum type draw texturing apparatus.

of the cone drum shape and other variables.

4. The yarn is in continuous contact with the friction surface of the cone drum.
5. The normal forces between the filament yarn and the cone drum in the false twisting contact region are constant.
6. The yarn maintains a circular cross-section of radius R.
7. Yarn bending moments, shear forces, and inertia forces are considered negligible in the false twisting contact region.

Calculation of Contact Angle for the False Twisting Contact Region

It is necessary to calculate the contact angle of the false twisting contact region for setting up the equilibrium equations.

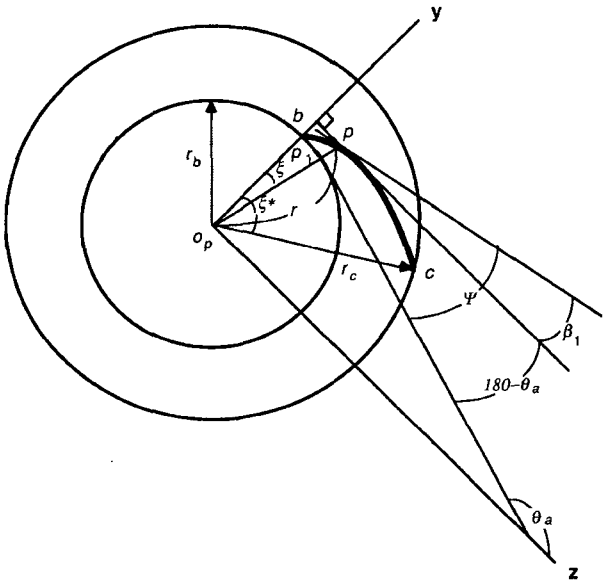

Figure 2. Relationship between the cone drum radius r and the projected angle ξ as seen perpendicular to the yz plain.

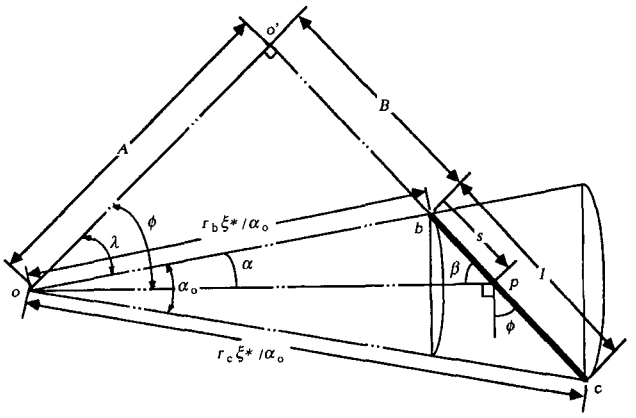

Figure 3. Relationship between the cone drum radius at any point and the length between the beginning point b and any point p on the false twisting region.

In order to calculate the contact angle we derive the relation between the cone drum radius r and the projected wrapping angle of b to p on the yz plane ξ first and foremost. Figure 2 illustrates the relationship between cone drum radius r and projected angle ξ as seen perpendicular to the yz plane.

In Figure 3 we obtain

$$\cos(\alpha+\lambda) = \frac{\overline{oo'}}{\overline{op}} \tag{1}$$

and

$$\overline{op} = \frac{\overline{oc}\cos(\alpha_o+\lambda)}{\cos(\alpha+\lambda)}. \tag{2}$$

On the other hand, from the proportional relation, $\alpha_o:\xi^* = \alpha:\xi$, we obtain

$$\alpha = \frac{\alpha_o}{\xi^*}\xi = \frac{r_b}{\overline{ob}}\xi = \frac{r_c}{\overline{oc}}\xi. \tag{3}$$

Substituting equation (2) into equation (1) we obtain

$$r = \frac{r_c\cos(\alpha_o+\lambda)}{\cos(\alpha+\lambda)}. \tag{4}$$

By inserting equation (3) into the above equation it follows that

$$r = C_1\sec(C_2\xi+\lambda) \tag{5}$$

where

$$C_1 = r_c\cos(\alpha_o+\lambda) = A\sin\frac{\alpha_c}{2} \tag{6}$$

$$C_2 = \frac{r_c}{\overline{oc}} = \sin\frac{\alpha_c}{2}. \tag{7}$$

Then by inserting the relations $\overline{oc}\cdot\alpha_0 = r_c\cdot\xi^*$ and $\alpha_o = \xi^*\sin\frac{\alpha_c}{2}$ into equation (5) it can be alternatively expressed as

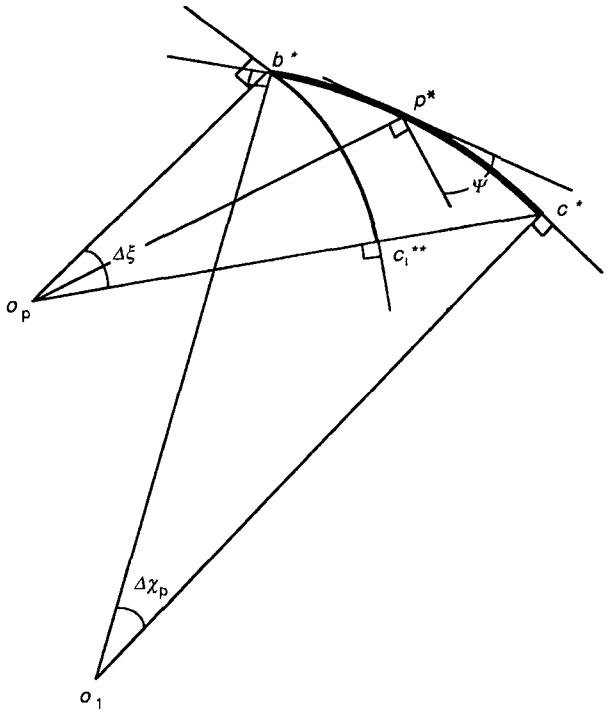

Figure 4. Projected freebody diagram of the element of the filament yarn in twisting zone.

$$r = \frac{r_c \cos\left(\xi^* \sin\frac{\alpha_c}{2} + \lambda\right)}{\cos\left\{\left(\sin\frac{\alpha_c}{2}\right)\xi + \lambda\right\}}. \tag{8}$$

In Figure 2, if we let the angle between two tangent lines drawn at point p and point p_1 be Ψ, then Ψ is equal to $(180 - \theta a) + \beta_1$. Since by using equation (5) we obtain

$$\Psi = \tan^{-1}\{C_2 \tan(C_2\xi + \lambda)\}. \tag{9}$$

By differentiating equation (9) with respect to ξ we obtain the result

$$d\Psi = \frac{C_2^2 \sec^2(C_2\xi + \lambda)}{1 + \{C_2 \tan(C_2\xi + \lambda)\}^2} d\xi. \tag{10}$$

Figure 4 illustrates the projected freebody diagram of the element of the filament yarn in twisting zone.

Let the projected contact angle of the element of false twisting region on the yz plane be $\Delta\chi_p$ then we may represent $\Delta\chi_p$ in the form of $\Delta\xi - \Delta\Psi$ where $\Delta\xi$ and $\Delta\Psi$ are increment of ξ and Ψ, respectively.

The element of false twisting region on the 3-D space is shown in Figure 5. This figure shows the freebody diagram of the element of the filament yarn in twisting zone. Let the true contact angle of the element of false twisting region be

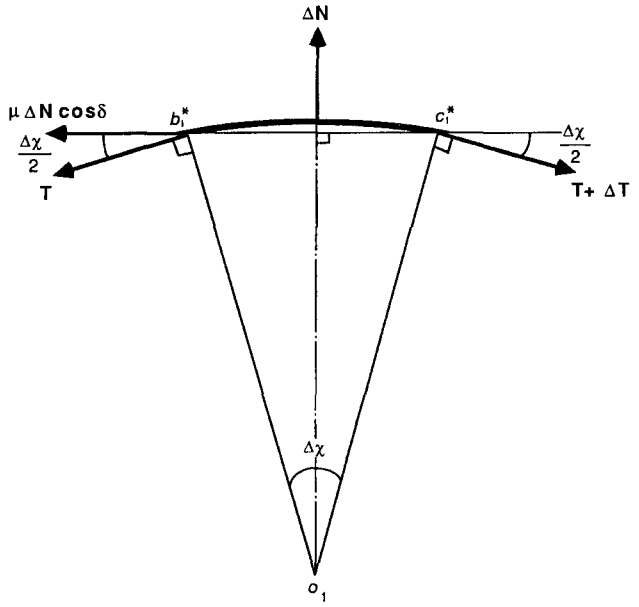

Figure 5. Freebody diagram of the element of the filament yarn in twisting zone.

$\Delta\chi$ in Figure 5.

Let the angle between the yarn axis and the cone drum axis be β then we can get the true contact angle for the $\Delta\xi$ region in Figure 5 as follows;

$$\Delta\chi = (\Delta\xi - \Delta\Psi)\sin\beta. \tag{11}$$

Therefore for $d\xi$ region the contact angle $d\chi$ is given by

$$d\chi = (d\xi - d\Psi)\sin\beta. \tag{12}$$

Calculation of Yarn Torque

An element of the filament yarn lying on the cone drum surface is shown in Figure 5. The normal reaction ΔN between the element of false twisting region and the cone drum surface is radial whilst the friction force $\mu\Delta N\cos\delta$ act tangentially to the contact line and resists the sliding of the element of false twisting region on the cone drum surface in Figure 5. The tension T and $T + \Delta T$ each subtend angle $\Delta\chi/2$ with the direction of the friction force.

The equations of equilibrium in this figure then are given as follows;

$$T\cos\frac{\Delta\chi}{2} + \mu\Delta N\cos\delta = (T + \Delta T)\cos\frac{\Delta\chi}{2} \tag{13}$$

and

$$T\sin\frac{\Delta\chi}{2} + (T + \Delta T)\sin\frac{\Delta\chi}{2} = \Delta N. \tag{14}$$

Hence by simplifying the above equations we obtain

$$\Delta T = \mu T\cos\delta(\Delta\xi - \Delta\Psi)\sin\beta \tag{15}$$

and if $\Delta\xi \rightarrow 0$

$$dT = \mu T\cos\delta(\xi)\{d\xi - d\Psi(\xi)\}\sin\beta(\xi). \quad (16)$$

Therefore, by integrating the above equation we obtain the result equation for the yarn tension T

$$T = T_2\exp\left\{\int_0^{\xi}\mu\cos\delta(\xi)\sin\beta(\xi)d\xi - \int_0^{\xi}\mu\cos\delta(\xi)\sin\beta(\xi)d\Psi(\xi)\right\}. \quad (17)$$

The axial torque generated by the friction of cone drum surface is given by

$$\Delta Q = \Delta TR\tan\delta \quad (18)$$

Substituting the relations between parameters in Figure 5 into the above equation we obtain

$$\Delta Q = \mu RT\Delta\chi\sin\delta \quad (19)$$

and by inserting equation (11), $\Delta\chi = (\Delta\xi - \Delta\Psi)\sin\beta$ into the above equation

$$\Delta Q = \mu RT\sin\delta(\Delta\xi - \Delta\Psi)\sin\beta \quad (20)$$

and if $\Delta\xi \rightarrow 0$ 0 then

$$dQ = \mu RT\sin\delta(\xi)\sin\beta(\xi)d\xi - \mu RT\sin\delta(\xi)\sin\beta(x)d\Psi(\xi). \quad (21)$$

By integrating equation (21) we obtain the result equation for the yarn torque Q

$$Q = \int_0^{\xi^*}\mu RT\sin\delta(\xi)\sin\beta(\xi)d\xi - \int_0^{\xi^*}\mu RT\sin\delta(\xi)\sin\beta(\xi)d\Psi(\xi). \quad (22)$$

Figures 6, 7, 8, and 9 show the plots of dimensionless

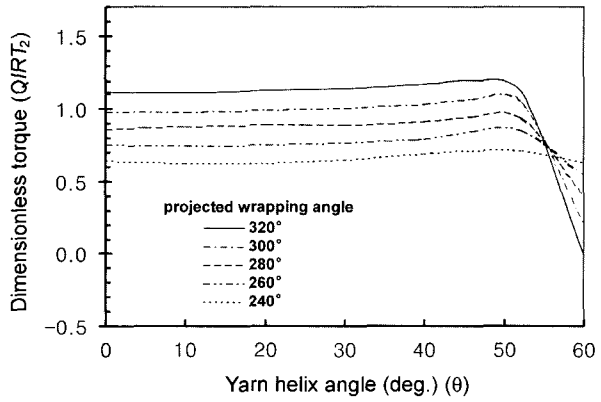

Figure 6. Plots of dimensionless torque Q/RT_2 versus yarn helix angle θ at various projected wrapping angles, for the conical angle of 0 °.

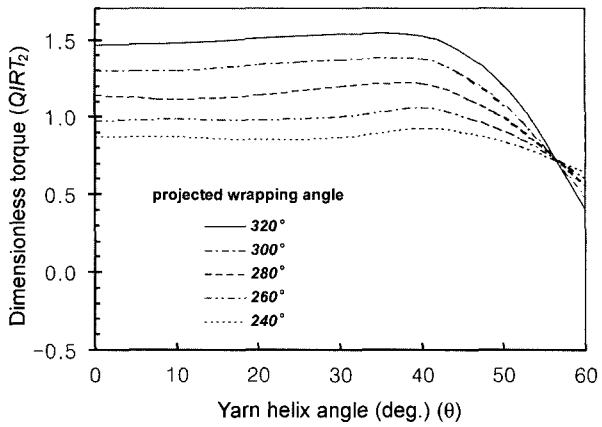

Figure 7. Plots of dimensionless torque Q/RT_2 versus yarn helix angle θ at various projected wrapping angles, for the conical angle of 10 °.

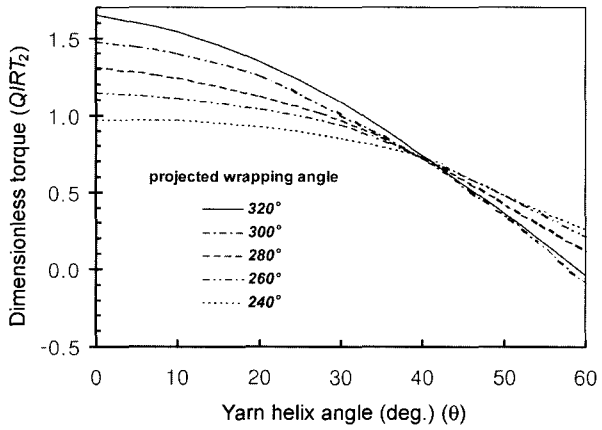

Figure 8. Plots of dimensionless torque Q/RT_2 versus yarn helix angle θ at various projected wrapping angles, for the conical angle of 22.62 °.

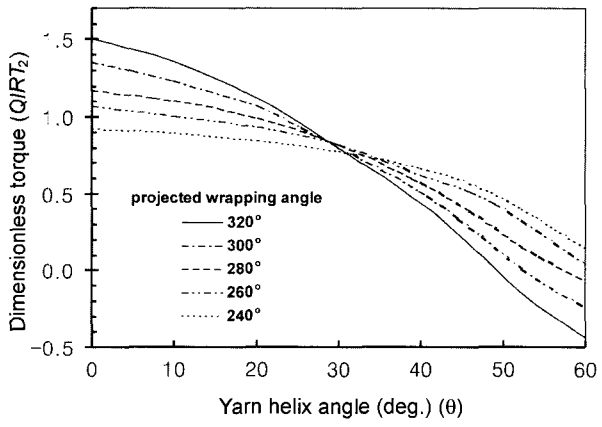

Figure 9. Plots of dimensionless torque Q/RT_2 versus yarn helix angle θ at various projected wrapping angles, for the conical angle of 30.75 °.

torque Q/RT_2 versus yarn helix angle θ at various projected wrapping angles and conical angles for the coefficient of friction μ of 0.31.

Experiments

The Newly Development Texturing Machine

The schematic diagram of the cone drum type draw texturing machine is shown in Figure 10. This apparatus has a pair of feed rollers, a heater for setting deformed yarn, a pair of cone drum twisters which forces yarn to rotate and a pair of take-up rollers. A filament yarn passes over the surface of the cone drum which rotates by the passing yarn without any special driving device.

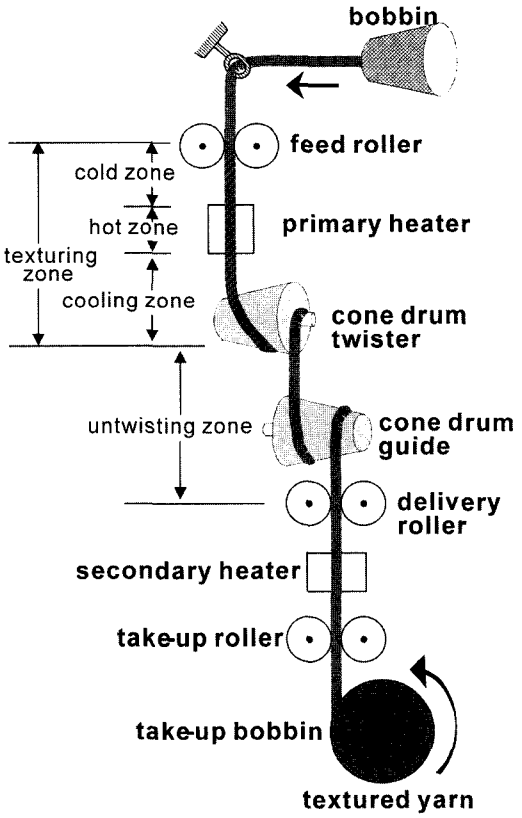

Figure 10. Schematic diagram of the cone drum type draw texturing machine.

Table 1. The specification of the cone drum

Minimum radius of the cone drum, r_b (mm)	6.0
Maximum radii of the cone drum, r_c (mm)	6.0, 9.5, 14.0, and 17.0
Length of the cone drum (mm)	40.0
Radius of the stud, r_d (mm)	4.0
Conical angle, α_c (deg.)	0.00, 10.00, 22.62, and 30.75

Table 2. Physical properties of polypropylene filament yarn

Linear density (den/fil)	103/24 POY yarn
Specific tenacity (g/den)	2.71
Breaking elongation (%)	142
Melting point (°C)	163
Skein shrinkage (%)	1.8
Fiber density (kg/m^3)	9×10^2

Table 3. The draw ratios and delivery speed for the experiment

Temperature	at room temperature
Draw ratio	1.4, 1.6, and 1.8
Delivery speed (m/min)	15.4

Specification of the Cone Drum

The specification of the cone drum used in the experiments is shown in Table 1.

Filament Yarn

Physical properties of polypropylene filament yarn used in the experiments are given in Table 2.

Experimental Conditions

Table 3 shows the draw ratios and delivery speed for the experiment.

Measurement of the Number of False Twist

The number of false twist was measured by the twister monitor (Model: TM-502, Toray) on the on-line system.

Measurement of the Yarn Torque for the False Twisting

The relation between the false twisting angle and the yarn torque was measured by Yarn Torsion and Intersecting Tester(type KES-YN-1), Kato Tech Co. Ltd.

Results and Discussion

Effect of Conical Angle of Cone Drum on the Dimensionless Torque

Figures 11, 12, and 13 show the effect of conical angle of cone drum on the dimensionless torque for various draw ratios such as 1.4, 1.6, and 1.8 respectively. The coefficient of friction for theoretical analysis is 0.31 which was evaluated experimentally for the take-up speed of 15.4 m/min.

In these figures the solid lines show the dimensionless torque Q/RT_2 which were calculated theoretically. The values of dimensionless torque increased up to the conical angle of 10 °, but it decreased upward of the conical angle of 22.62 °. We can trace the origin of these phenomena in Figures 6, 7, 8, and 9.

In Figure 6, for the conical angle of 0 °, the dimensionless

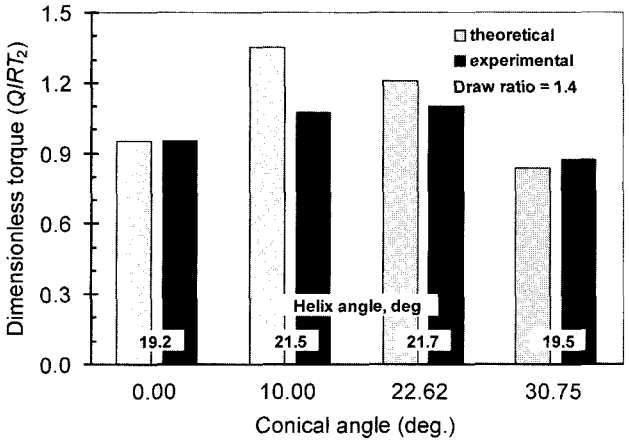

Figure 11. Effect of conical angle on the dimensionless torque for the draw ratio of 1.4.

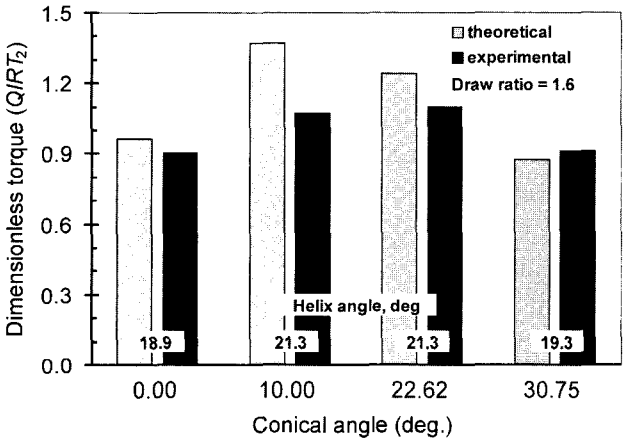

Figure 12. Effect of conical angle on the dimensionless torque for the draw ratio of 1.6.

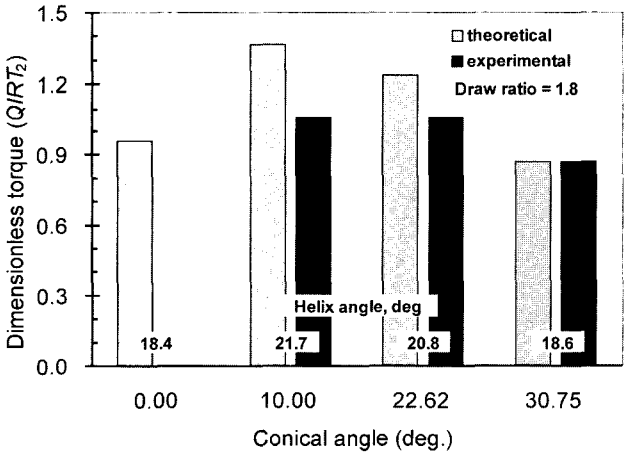

Figure 13. Effect of conical angle on the dimensionless torque for the draw ratio of 1.8.

torque increased slightly upto the twist angle of 50°, but it decreased radically upward of the twist angle of 50°. This is caused by the change of drag angle. And if we make a comparison between Figures 6, 7, 8, and 9 reciprocally, we see that the initial dimensionless torque increased with the increase of the conical angle, but it decreased at the conical angle of 30.75°. This is owing to the reason of increase of $\sin\beta$ with the increase of the conical angle. But when the angle reached 30.75° the dimensionless torque decreased owing to increase of $d\Psi/d\xi$.

On the other hand, in Figures 6, 7, 8, and 9 the dimensionless torque decreased more and more radically with the increase of the conical angle. This is owing to the increase of $d\Psi/d\xi$ with the increase of the conical angle.

Therefore putting all these accounts together we can explain the phenomena of Figures 11, 12, and 13 as follows; up to the conical angle of 10°, the dimensionless torque increased owing to the dominant effect of the increase of the contact length and $\sin\beta$. But the increase of the conical angle above the conical angle of 10° the dimensionless torque decreased owing to the dominant effect of decreasing of contact angle.

The experimental values of the dimensionless torque also increased at the early stage with the increase of the conical angle but it decreased when the conical angle increased more and more. At the early stage owing to the dominant effect of increase of the contact length the dimensionless torque also increased, but owing to the dominant effect of the decreasing of contact angle, it decreased for the latter part.

The differences between theoretical prediction and performed experiments at the conical angles of 10° and 22.62° are owing to the assumptions for simplifying the equations, i.e., the assumptions of the shortest path in the false twisting contact region, the constant coefficient of friction, the circular cross-section yarn, and neglecting yarn bending moments, shear forces, and inertia forces are the cause of differences.

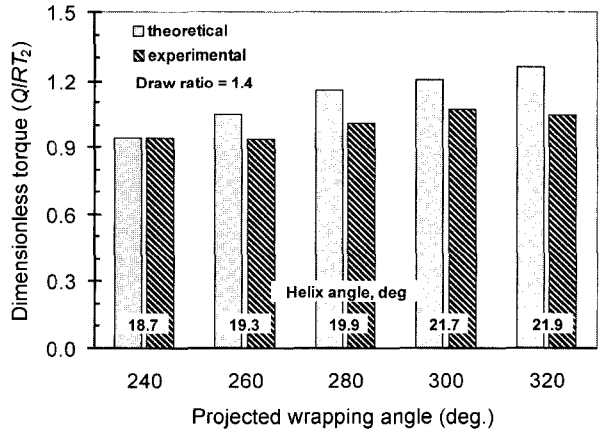

Figure 14. Effect of projected wrapping angle of false twisting zone on the dimensionless torque for the draw ratio of 1.4.

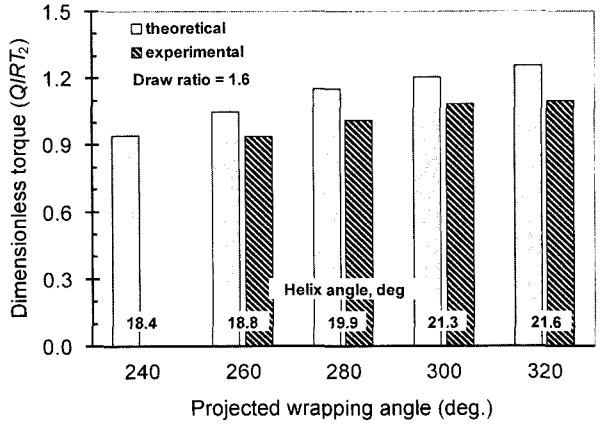

Figure 15. Effect of projected wrapping angle of false twisting one on the dimensionless torque for the draw ratio of 1.6.

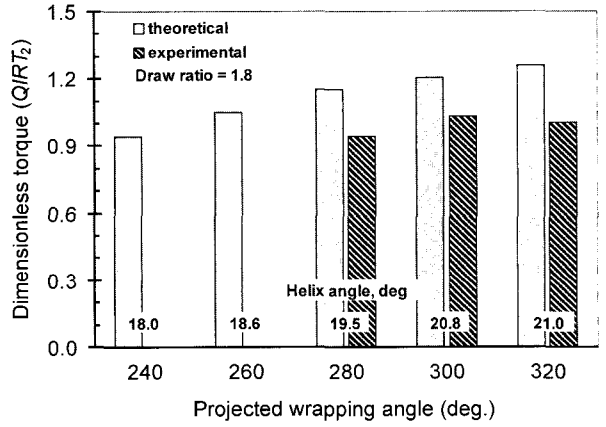

Figure 16. Effect of projected wrapping angle of false twisting zone on the dimensionless torque for the draw ratio of 1.8.

Effect of Projected Wrapping Angle of False Twisting Zone on the Dimensionless Torque

Figures 14, 15, and 16 show the effect of the projected wrapping angle of false twisting zone ξ^* on the dimensionless torque Q/RT_2 under the conical angle of 22.62 ° for the draw ratio of 1.4, 1.6, and 1.8 respectively. The coefficient of friction for theoretical analysis is 0.31 which was evaluated experimentally for the take-up speed of 15.4 m/min.

In these figures the solid lines show the dimensionless torque Q/RT_2 which were calculated theoretically. The values of dimensionless torque increased with the increase of the projected wrapping angle of false twisting zone ξ^*. This phenomena can explain by Figure 8 in which the dimensionless torque increased with the increase of the projected wrapping angle of the false twisting zone up to the angle of 42 °-43 ° but it decreased upward of the projected wrapping angle of the false twisting zone up to the angle of 42 °-43 °. Owing to the dominant effect of increase of the drag angle and decrease of the contact angle, the dimensionless torque decreased in Figure 8. The values of dimensionless torque increased with the increase of the projected wrapping angle of the false twisting zone in Figures 14, 15, and 16 because the false twist angles are within the range of 18 °-22 ° in Figure 8.

The experimental values in Figures 14, 15, and 16 also increased with the increase of the projected wrapping angle of the false twisting zone owing to the increase of the contact length.

The values of dimensionless torque in both theoretical prediction and performed experiments have a tendency of increase. But an increasing rate of experimental values is lower than that of theoretical prediction values. The differences between theoretical prediction and performed experiments are owing to the assumptions for simplifying the equations. The assumptions of the shortest path in the false twisting contact region, the constant coefficient of friction, the circular cross-section yarn, and neglecting yarn bending moments, shear forces, and inertia forces are the cause of differences.

Conclusions

Newly developed cone drum twister texturing mechanism was investigated theoretically and experimentally. Through the analysis of the dimensionless torque in false twisting mechanism the following results were obtained.

The cone drum twister can be classified as one of the outer surface contacting friction-twisting devices in false-twist texturing. An analysis is given from which equations can be derived that relate the conical angle of cone drum, wrapping angle, drag angle, and yarn helix angle. Theoretical values of dimensionless torque were calculated and were compared with the experimental values obtained at room temperature. It is shown that, as the conical angle increased, the dimensionless torque also increased both theoretically and experimentally. But over the 10° of the conical angle, the dimensionless torque decreased. And it is also shown that, as the projected wrapping angle increased, the dimensionless torque also increased both theoretically and experimentally.

Nomenclature

α : Angle between *ob* and *op* in the opening out diagram
α_c : Conical angle of cone drum
α_o : Angle between *ob* and *oc* in the opening out diagram
β : Angle between the yarn axis and the cone drum axis
δ : Angle between the drag velocity and the filament yarn axis
ζ : Drag velocity of the friction surface relative to the yarn surface
θ : Surface helix angle of the filament yarn in twisting zone
λ : Angle between *ob* and *oo'*
μ : Friction coefficient
ξ : Angle of wrap(*bp* region) on the friction surface as

seen perpendicular to the *yz* plane
ξ^* : Angle of wrap(*bc* region) on the friction surface as seen perpendicular to the *yz* plane
ϕ : Angle between the filament yarn axis and the direction of friction surface movement
χ : True angle of wrap
Ψ : Angle between tangent at point *p* and tangent at point *p'* as seen perpendicular to the *yz* plane
ω : Angular velocity of cone drum [rad/sec]
A : Length of *oo'* [mm]
B : Length of *bo'* [mm]
b : Beginning point of false twist inserting
C_1 : A $\sin(\alpha_c/2)$ [mm]
C_2 : $\sin(\alpha_c/2)$
c : End point of false twist inserting
D : Velocity of friction surface [mm/sec]
D_b : Velocity of friction surface at point *b* [mm/sec]
D_c : Velocity of friction surface at point *c* [mm/sec]
$\bar{e}$: Mean length of filaments in the length *h* of twisted yarn [mm]
h : Length of one turn of twist [mm]
K : Ratio of cone drum surface speed to forward yarn speed($=D/V_1$)
l : Length of filament yarn in twisting zone, *bc* [mm]
l_o : Length of *bc* in the flat drum [mm]
N : Normal force of the filament yarn on the surface of drum [g_f]
n : Number of filaments crossing unit area perpendicular to the filament axis
p : Any point on the line *bc*
Q : Torque supplied to the filament yarn in twisting zone, *bc* [$g_f \cdot$ mm]
R : Radius of the filament yarn [mm]
r : Cone drum radius at any point [mm]
r_b : Cone drum radius at point *b* [mm]
r_c : Cone drum radius at point *c* [mm]
r_d : Radius of the stud of cone drum [mm]
s : Length of *bp* [mm]
T : Yarn tension [g_f]
T_1 : Output tension at point *c* [g_f]
T_2 : Input tension at point *b* [g_f]
V_o : Forward velocity of the zero twist filament yarn [mm/sec]
V_1 : Forward velocity of the twisted filament yarn in twisting zone [mm/sec]
V_2 : Circumferential velocity resulting from twisting of filament yarn in twisting zone [mm/sec]
V_i : Forward velocity of the filament yarn containing the twist angle, θi [mm/sec]
V_R : Surface velocity of the twisted filament yarn [mm/sec]

References

1. T. J. Kang, *Text. Res. J.*, **58**, 653 (1988).
2. J. J. Thwaites, *J. Textile Inst.*, **76**, 157 (1985).
3. W. J. Morris and M. J. Denton, *J. Textile Inst.*, **66**, 123 (1975).
4. H. G. Howell, *J. Textile Inst.*, **44**, T359 (1953).
5. J. J. Theaites, *J. Textile Inst.*, **75**, 285 (1984).
6. M. J. Denton, *J. Textile Inst.*, **66**, 80 (1975).
7. C. G. Lee, Ph. D. Dissertation, Seoul National University, Seoul, 1993.
8. C. G. Lee and T. J Kang, *J. Kor. Fiber Soc.*, **33**, 248 (1996).
9. C. G. Lee and T. J Kang, *J. Kor. Fiber Soc.*, **33**, 393 (1996).
10. C. G. Lee, *J. Kor. Fiber Soc.*, **32**, 621 (1995).
11. C. G. Lee, *J. Kor. Soc. Cloth.. Ind.*, **2**, 443 (2000).
12. C. G. Lee, *J. Kor. Soc. Cloth.. Ind.*, **3**, 473 (2001).